



Grain boundary blocking of ionic conductivity in nanocrystalline yttria-doped ceria thin films

Jihwan An,^{a,1} Jiwoong Bae,^{b,1} Soonwook Hong,^b Bongjun Koo,^b Young-Beom Kim,^{b,e,*} Turgut M. Gür^d and Fritz B. Prinz^{c,d}

^aManufacturing Systems and Design Engineering (MSDE) Program, Seoul National University of Science and Technology, Seoul 139-743, Republic of Korea

^bDepartment of Mechanical Convergence Engineering, Hanyang University, Seoul 133-791, Republic of Korea

^cDepartment of Mechanical Engineering, Stanford University, Stanford, CA 94305, USA

^dDepartment of Materials Science and Engineering, Stanford University, Stanford, CA 94305, USA

^eInstitute of Nano Science and Technology, Hanyang University, Seoul 133-791, Republic of Korea

Received 5 December 2014; revised 9 March 2015; accepted 30 March 2015

Available online 14 April 2015

Nanocrystalline YDC thin films with grain-sizes ranging from 38 to 93-nm were prepared using pulsed laser deposition followed by thermal annealing. Ionic conductivity decreased up to four orders of magnitude as the grain size increased. Using energy-dispersive X-ray spectroscopy, we showed that the counter-intuitive reduction in conductivity with grain-size is likely due to dopant and impurity segregation near grain-boundaries. Spectroscopic evidence suggests that the blocking effect due to defect segregation is more dominant on ionic conductivity than the grain-sizes. © 2015 Acta Materialia Inc. Published by Elsevier Ltd. All rights reserved.

Keywords: Yttria-doped ceria; Grain boundaries; Ionic conductors; Nanocrystalline materials; Solid oxide fuel cell

Nanocrystalline materials have unusual and exceptional electrical and chemical properties [1–3], some of which are due to their nanoscale grain sizes and highly dense grain boundaries. Compared to bulk materials, nanocrystalline films used in solid oxide fuel cells have an extremely high density of grain boundaries, and therefore, understanding the role of grain boundaries in ion transport is crucial [4–9].

There is evidence that grain boundaries affect the electrochemical properties and behavior of thin film solid oxide fuel cell (SOFC) components in two main ways. First, in terms of cathode interfacial kinetics, grain boundaries at the external surface of the solid oxide electrolyte, e.g., yttria-stabilized zirconia (YSZ), exhibit a higher surface exchange coefficient for oxygen than the bulk [10–17]. Due to dopant segregation, grain boundaries contain a higher population of oxygen vacancies than the bulk, and thus facilitate low activation energy for oxygen incorporation [14–16]. Second, previous work studying the effects of dopant distribution, space charge, as well as grain size on ionic transport across grain

boundaries revealed that grain boundary resistivity is usually several orders higher than that of the bulk [18–22]. Thus, understanding the blocking effect of grain boundaries on ionic conductivity in nanocrystalline materials requires a study of how grain size and thermal history affect ion transport in nanocrystalline films.

Yttrium-doped ceria (YDC) is a promising electrolyte material for low temperature solid oxide fuel cells (LT-SOFCs) because of its superior ionic conductivity and lower activation energy for ionic transport than YSZ, which is the electrolyte material most commonly used in SOFCs [5,23]. Previous studies on nanocrystalline YDC examined the effects of grain size on ionic conductivity by varying the grain size using different thermal conditions to generate different grain boundary densities [1,4,6,20,24,25]. However, even though the effects of heat treatment on grain boundary density were considered in these studies, the effects of heat treatment on dopant segregation were not.

With this in mind, we investigated the effects of grain size and dopant distribution on grain boundary blocking of ionic conductivity in nanocrystalline YDC films. Through spectroscopic study and electrochemical analysis, we conclude that not only grain-boundary density, but also dopant segregation is affected by thermal treatment, which strongly influences the ionic conductivity of the films.

* Corresponding author at: Department of Mechanical Convergence Engineering, Hanyang University, Seoul 133-791, Republic of Korea. Tel.: +82 2 2220 0544; fax: +82 2 2220 2299.; e-mail: ybkim@hanyang.ac.kr

¹These authors contributed equally to this work.

Nanocrystalline YDC films were deposited on a quartz substrate by pulsed laser deposition (PLD) at a substrate temperature of 750 °C. A Lambda Physik 248 nm KrF excimer laser with an energy density of 1.5 J/cm² per pulse was applied to a sintered Y_{0.1}Ce_{0.9}O₂ target. The sample-to-target distance was 50 mm, and PLD deposition was conducted under 100 mTorr of oxygen gas pressure. As a result, 200 nm-thick YDC films were grown with a nominal growth rate of 0.22 Å/pulse.

To systematically control the grain size and thermal history of the YDC film, as-deposited nanocrystalline YDC films were post-annealed at 1000 °C and 1200 °C for 10 h. Post-annealing was conducted in an electric furnace under ambient air ($P_{O_2} = 0.21$ atm) with a ramping rate of 40 °C/min. Surface topography of YDC films was investigated using AFM in non-contact surface scanning mode. Chemical composition of the prepared YDC films was investigated by X-ray photoelectron spectroscopy (XPS).

After heat treatment, platinum electrode pads (700 μm × 700 μm in size and spaced 300 μm apart) were deposited on the top surface of the 200 nm-thick YDC films by DC sputtering for electrochemical analysis. Nanocrystalline YDC film samples with different grain sizes and thermal histories were mounted on a temperature-controlled heating stage for ionic conductivity measurements. Electrochemical impedance spectroscopy (EIS) was carried out using an electrochemical analyzer (Gamry Potentiostat FAS2, Gamry Instruments, Inc.) under 0 V and 1 V dc bias. EIS measurements were performed in the frequency range of 300 kHz to 0.5 Hz and between 320 °C and 550 °C. Measured impedance data were fitted using Nyquist plots through the equivalent circuit model, and Faradaic impedances were extracted at different temperatures to obtain the activation energy for ionic conduction.

To prepare TEM-EDS samples, 50 nm of nanocrystalline YDC films were deposited on a TEM grid using the same PLD conditions mentioned above. After deposition, an annealing process was conducted at 1200 °C for 10 h on one of the two TEM samples to distinguish the morphological and stoichiometric differences between as-deposited- and 1200 °C-annealed YDC films. Areas near the Y-Kα (14.96 keV) and Ce-Kα (34.72 keV) peaks were integrated to compare the compositions of grain boundary and grain center regions. TEM-EDS measurements were conducted with a probe size of approximately 5 nm.

Grain structures of the as-deposited and annealed films (50 nm in thickness) were investigated by TEM (Fig. 1). As-deposited YDC film had an average grain size of approximately 10 nm in diameter, while grain size increased to approximately 50 nm in diameter in YDC film annealed at 1200 °C for 10 h, due to the grain growth mechanism.

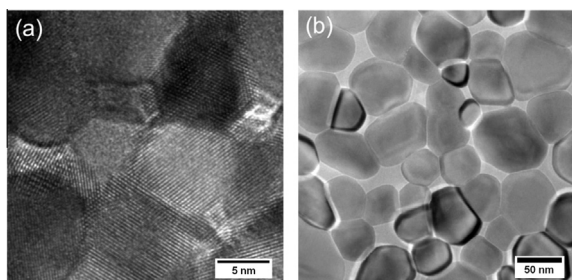


Figure 1. Plan-view TEM images of (a) as-deposited and (b) annealed (10 h at 1200 °C) YDC films (50 nm in thickness).

TEM images also revealed that both films consisted of vertically columnar grain structures. The formation of columnar-structured film, which is facilitated by fast surface diffusion, has been reported previously by other researchers who used similar experimental conditions [3].

We conducted TEM-EDS of the as-deposited and annealed (10 h at 1200 °C) films to investigate the ratio of dopant (Y³⁺) concentration at the grain boundary and the grain center region according to heat treatment (Fig. 2). As expected, the normalized site ratio for the Ce⁴⁺ ions with respect to the grain center versus the grain boundary region in the as-deposited and annealed samples are nearly the same. By contrast, however, the normalized site ratio for Y³⁺ at the grain boundary region to that at the grain center region in the as-deposited YDC film was 0.94 ± 0.10 , while that in the 1200 °C-annealed sample was 1.46 ± 0.25 . This clearly shows preferential segregation of Y³⁺ to grain boundaries. The uniform distribution of Y³⁺ concentration in the as-deposited film suggests lack of favorable conditions to drive dopant segregation to the grain boundary region. On the other hand, dopant segregation at the grain boundary was significant in the annealed film. We hypothesize that the thermal energy provided by annealing induces not only grain growth, but also segregation of dopants near grain boundaries by providing enough energy for dopant mobility [15,16,26,27].

The role of defect segregation on ionic conductivity was further studied by EIS measurements. Three samples (200 nm in thickness) were prepared: an as-deposited sample (deposited at 750 °C), and two samples annealed at 1000 °C and at 1200 °C for 10 h, respectively. AFM images of the three samples are shown in Figure 3a–c. Grain sizes of the as-deposited, 1000 °C-annealed, and 1200 °C-annealed YDC films were 38 ± 2 nm, 68 ± 6 nm, and 93 ± 6 nm, respectively.

EIS was conducted under 0 V and 1 V dc bias conditions, and in the frequency range from 300 kHz to 0.5 Hz. Representative Nyquist plots for the as-deposited YDC

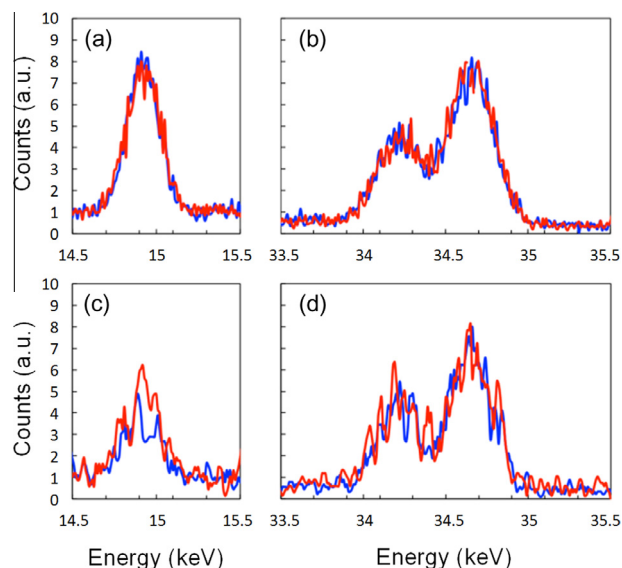


Figure 2. EDS spectra of YDC samples near (a) the Y-Kα edge and (b) the Ce-Kα edge in the as-deposited sample, and (c) the Y-Kα edge and (d) the Ce-Kα edge in the annealed sample. Spectra in red are from grain boundaries, and those in blue are from grain centers. (For interpretation of the references to color in this figure legend, the reader is referred to the web version of this article.)

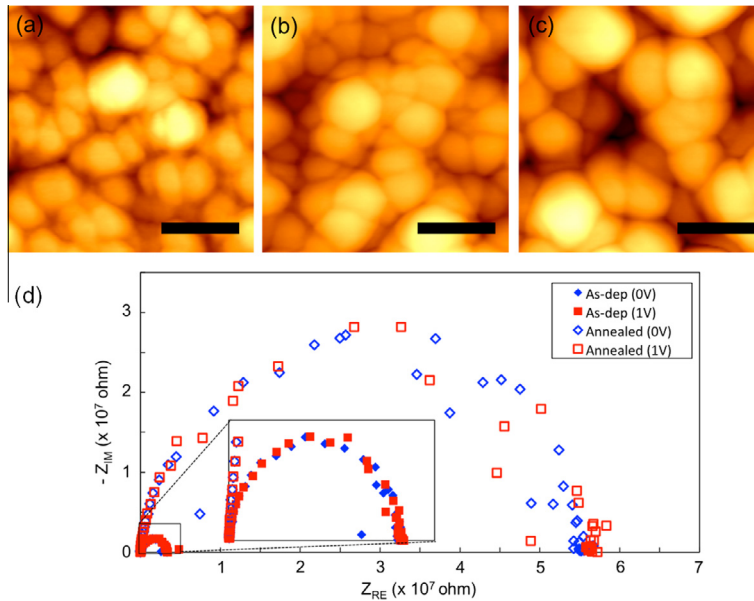


Figure 3. AFM images of 200 nm-thick YDC films: (a) as-deposited, (b) annealed at 1000 °C, and (c) annealed at 1200 °C. Scale bars are 100 nm. (d) Sample EIS spectra of as-deposited and 1000 °C-annealed YDC films at 0 V and 1 V. Inset is the zoomed-in plot for $0 < Z_{RE} < 4E6$ (ohm), and $0 < -Z_{IM} < 2E6$ (ohm).

film and 1000 °C-annealed film measured at 500 °C are shown in Figure 3d. In both EIS spectra, one semicircle independent of bias conditions was observed, representing the contribution from ionic transport inside the electrolyte [28,29]. However, it was not possible to discern the individual contributions from the bulk and the grain boundaries in the spectra.

Ionic conductivity and activation energy were evaluated by the Arrhenius relation based on EIS data measured between 320 °C and 550 °C (Fig. 4). Two interesting observations were made from the Arrhenius plot: (1) the ionic conductivity and activation energy of the as-deposited sample were comparable to those of epitaxial YDC, and (2) the ionic conductivity decreased while the activation energy increased in the annealed samples; the ionic conductivity decreased more when the sample was annealed at a higher temperature.

First, it is notable that the as-deposited film had similar ionic conductivity and activation energy (0.97 eV) as the epitaxial or bulk YDC film, even though it had the smallest

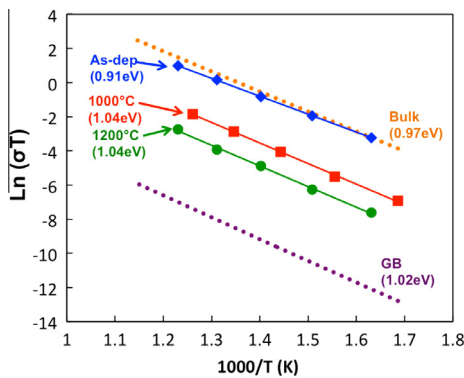


Figure 4. Arrhenius plot of as-deposited, 1000 °C-annealed, and 1200 °C-annealed samples (12 mol% YDC). Reference data for dotted-lines, which represent the bulk (i.e., epitaxial), and grain-boundary conductivities for 10 mol% YDC are from Ref. [19].

grains (highest grain-boundary density) among all three samples. The ionic conductivity of the as-deposited nanocrystalline film was also comparable to that of microcrystalline films reported elsewhere even though the density of the grain-boundary is even higher in nanocrystalline film (e.g., two orders of magnitude denser than microcrystalline film (average grain size $\sim 1\text{--}2.5$ μm)) [20,23,30,31]. Furthermore, in the nanocrystalline-doped ceria film fabricated under similar deposition conditions (650 °C, 1 h), oxygen vacancies are reported to be preferentially associated with Ce^{4+} ions than with Y^{3+} ions, i.e., oxygen vacancies are distributed more uniformly, which may enhance vacancy hopping and therefore ionic conductivity [33]. This mechanism may have also contributed to the relatively high ionic conductivity of the as-deposited film.

Another notable point is that the ionic conductivity of the nanocrystalline YDC film sharply dropped by one to two orders of magnitude and the activation energy increased by ~ 0.1 eV after it was annealed at 1000–1200 °C for 10 h. This is despite the fact that the grain boundary density decreased due to grain growth, e.g., 43% decrease in 1000 °C-annealed and 59% decrease in the 1200 °C-annealed films compared to as-deposited film (determined from AFM images). Indeed, the ionic conductivity of the YDC film approached that of the grain boundary conductivity when the film was annealed: that is, ionic conduction at the grain-boundary regions seems to dominate the overall ionic transport. A similar trend (i.e., the higher ionic conductivity of fine-grained YDC (low sintering temperature) than coarse-grained YDC (high sintering temperature)) has been also previously reported in several papers [26,34]. For instance, Tian and Chan reported that YDC sintered at 1400 °C shows higher DC conductivity than YDC sintered at 1500 °C [26]. They argued that the larger density of grain-boundaries due to the finer grain size provides more room for solutes to segregate in the 1400 °C sample than in the 1500 °C sample. Moreover, the low mobility of dopant ions in a sample sintered at low temperature may have impeded the formation of grain-

boundary structure (i.e., grain-boundary core and space charge layers). Bellino et al. also pointed out that the increase of ionic conductivity in fine-grained YDC may be due to the transition of ionic transport mechanism from brick layer model to parallel model: that is, the ionic conduction along grain-boundaries, which is faster than that in the bulk or across grain-boundaries, becomes dominant because the volume fraction of grain boundaries becomes comparable to that of bulk [4,32,34]. Also in such fine-grained nanocrystalline materials, neighboring space charge layers may overlap, and thus the individual grains lose their bulk properties [4,32]. Moreover, Sen et al. experimentally showed that oxygen vacancies preferentially associate with Y^{3+} ions rather than with Ce^{4+} ions in YDC films treated at 1400 °C for 12 h [33], which implies that segregation of dopant ions may have induced even more significant segregation of oxygen vacancies at the grain boundary in our annealed films. High local concentration of oxygen vacancies may induce interactions among them resulting in the generation of extended defects, which may further decrease ionic conductivity [35].

Furthermore, the lower ionic conductivity of the 1200 °C-annealed sample than that for the 1000 °C-annealed sample may also be due to silicon (found to be <0.1 at.% and <5 at.% in the 1000 °C-annealed films and in the 1200 °C-annealed films, respectively, by XPS measurement) diffusion from the substrate preferentially along grain boundaries [18,20].

The extent of individual contributions of each of these factors to the observed ionic conductivity in YDC, however, is still unresolved at this point. We are currently investigating this topic in more detail in our laboratory.

In summary, the blocking effect of the grain boundary on ionic conduction in nanocrystalline YDC films was investigated with different grain sizes and thermal histories. After post-annealing, dopant segregation at the grain boundaries became significant while it was not observed in as-deposited YDC film. Concentration of oxygen vacancies due to dopant segregation may hinder ionic transport by a space charge layer effect, decreasing the ionic conductivity of annealed YDC films. As-deposited YDC film showed comparable ionic conductivity and activation energy to epitaxial YDC film, but ionic conductivity decreased as the annealing temperature increased. Spectroscopic evidence presented in this study suggests that dopant segregation has a more pronounced impact on ionic conductivity than grain size, i.e., grain boundary density.

Y.B.K. gratefully acknowledges financial support from the National Research Foundation (NRF) of the Korean Ministry of Education, Science, and Technology (MEST) (Grant No. NRF-2014R1A1A2060078). J.A., T.M.G., and F.B.P. gratefully acknowledge partial support from the Center on Nanostructuring for Efficient Energy Conversion (CNEEC) at Stanford University, an Energy Frontier Research Center funded by the U.S. Department of Energy, Office of Science, Office of Basic Energy Sciences under Award Number DE-SC0001060.

- [1] J.L.M. Rupp, L.J. Gauckler, *Solid State Ionics* 177 (2006) 2513.
 [2] J.H. Shim, C.C. Chao, H. Huang, F.B. Prinz, *Chem. Mater.* 19 (2007) 3850.

- [3] D. Beckel, A. Bieberle-Hütter, A. Harvey, A. Infortuna, U.P. Muecke, M. Prestat, J.L.M. Rupp, L.J. Gauckler, *J. Power Sources* 173 (2007) 325.
 [4] H.L. Tuller, *Solid State Ionics* 131 (2000) 143.
 [5] B.C.H. Steele, *Solid State Ionics* 75 (1995) 157.
 [6] A. Tschöpe, E. Sommer, R. Birringer, *Solid State Ionics* 139 (2001) 255.
 [7] Y. Chem, S. Omar, A.K. Keshri, K. Balani, K. Babu, J.C. Nino, S. Seal, A. Agarwal, *Scr. Mater.* 60 (2009) 1023.
 [8] H. Hojo, T. Mizoguchi, H. Ohta, S.D. Findlay, N. Shibata, T. Yamamoto, Y. Ikuhara, *Nano Lett.* 10 (2010) 4668.
 [9] M. Shirpour, B. Rahmati, W. Sigle, P.A. van Aken, R. Merkle, J. Maier, *J. Phys. Chem. C* 116 (2012) 2453.
 [10] R.A.D. Souza, M.J. Pietrowski, U. Anselmi-Tamburini, S. Kim, Z.A. Munir, M. Martin, *Phys. Chem. Chem. Phys.* 10 (2008) 2067.
 [11] Y.B. Kim, T.P. Holme, T.M. Gür, F.B. Prinz, *Adv. Funct. Mater.* 21 (2011) 4684.
 [12] Y.B. Kim, J.S. Park, T.M. Gür, F.B. Prinz, *J. Power Sources* 196 (2011) 10550.
 [13] J.H. Shim, J.S. Park, T.P. Holme, K. Crabb, W. Lee, Y.B. Kim, X. Tian, T.M. Gür, F.B. Prinz, *Acta Mater.* 60 (2012) 1.
 [14] J.S. Park, T.P. Holme, J.H. Shim, F.B. Prinz, *MRS Commun.* 2 (2012) 107.
 [15] J. An, J.S. Park, A.L. Koh, H.B. Lee, H.J. Jung, J. Schoonman, R. Sinclair, T.M. Gür, F.B. Prinz, *Sci. Rep.* 3 (2013) 2680.
 [16] J. An, A.L. Koh, J.S. Park, R. Sindair, T.M. Gür, F.B. Prinz, *J. Phys. Chem. Lett.* 4 (2013) 1156.
 [17] S.B. Adler, *Chem. Rev.* 104 (2004) 4791.
 [18] X. Guo, J. Maier, *J. Electrochem. Soc.* 148 (2001) E121.
 [19] J.S. Park, Y.B. Kim, J. An, F.B. Prinz, *Solid State Commun.* 152 (2012) 2169.
 [20] X. Guo, W. Sigle, J. Maier, *J. Am. Ceram. Soc.* 86 (2003) 77.
 [21] O.J. Durá, M.A. López de la Torre, L. Vázquez, J. Chaboy, R. Boada, A. Rivera-Calzada, J. Santamaria, C. Leon, *Phys. Rev. B* 81 (2010) 184301.
 [22] S. Kim, J. Maier, *J. Electrochem. Soc.* 149 (2002) J73.
 [23] H.B. Wang, H.Z. Song, C.R. Xia, D.K. Peng, G.Y. Meng, *Mater. Res. Bull.* 35 (2000) 2363.
 [24] E.C.C. Souza, W.C. Chueh, W. Jung, E.N.S. Muccillo, S.M. Haile, *J. Electrochem. Soc.* 159 (2012) K127.
 [25] F. Maglia, I.G. Tredici, U. Anselmi-Tamburini, *J. Eur. Ceram. Soc.* 33 (2013) 1045.
 [26] C. Tian, S.W. Chan, *Solid State Ionics* 134 (2000) 89.
 [27] W. Lee, H.J. Jung, M.H. Lee, Y.B. Kim, J.S. Park, R. Sinclair, F.B. Prinz, *Adv. Funct. Mater.* 22 (2012) 965.
 [28] R. O'Hayer, S.W. Cha, W. Colella, F.B. Prinz, *Fuel Cell Fundamentals*, second ed., John Wiley & Sons, New York, 2009.
 [29] E. Barsoukov, J.R. Macdonald, *Impedance Spectroscopy: Theory, Experiment, and Applications*, second ed., John Wiley & Sons, New York, 2005.
 [30] X. Guo, R. Waser, *Prog. Mater. Sci.* 51 (2006) 151.
 [31] Y. Gu, G. Li, G. Meng, D. Peng, *Mater. Res. Bull.* 35 (2000) 297.
 [32] J. Maier, *Solid State Ionics* 23 (1987) 59.
 [33] S. Sen, H.J. Avila-Paredes, S. Kim, *J. Mater. Chem.* 18 (2008) 3915.
 [34] M.G. Bellino, D.G. Lamas, N.E. Walsöe de Reca, *Adv. Funct. Mater.* 16 (2006) 107.
 [35] A. Nakamura, J.B. Wagner Jr., *J. Electrochem. Soc.* 133 (1986) 1542.